Crystallization Behavior of PA-6 Clay Nanocomposite Hybrid

Eric Devaux, Serge Bourbigot, Ahmida El Achari

Laboratoire de Génie et Matériaux Textiles (GEMTEX), UPRES EA2461, Ecole Nationale Supérieure des Arts et Industries Textiles (ENSAIT), BP 30329, 59056 Roubaix Cedex 01, France

ABSTRACT: Polyamide-6 (PA-6)/clay (modified montmorillonite) hybrid was synthesized by melt blending at high shear stress. ^{27}Al-NMR of solid state shows that the clay is not modified after melt blending. Using wide-line ^{1}H-NMR and TEM, it is demonstrated that the nanocomposite exhibits mainly an exfoliated structure. It is shown that the modified montmorillonite induces the crystallization of PA-6 predominantly in γ-form. The presence of clay in PA-6 increases the polymer crystallization temperature, and decreases its melting point. These phenomena show that a certain number of interactions develop near the reinforcing material, and that the latter plays a particular role of nucleating agent. However, the crystallization is not spherulitic and the assumption of macromolecular orientation in the vicinity of the clay is demonstrated by the observations carried out in DSC and AFM. These particular properties of orientation will have a particular importance on the mechanical behavior of the nanocomposite material. © 2002 Wiley Periodicals, Inc. J Appl Polym Sci 86: 2416–2423, 2002

Key words: nanocomposites; polyamides; crystallization

INTRODUCTION

Polyamide resins are widely used as injected and extruding molded materials and in the textile industry. They have been successfully reinforced using glass fibers and other inorganic additives.[1] Nevertheless, in such composites, the polymer and the additives are not homogeneously dispersed. To overcome this problem and to improve the properties of the host polymer, molecular composite of thermoplastics was synthesized. The studies on nanocomposites began in the early 1980s at Toyota Central Research Laboratories.[2] The first licensee of Toyota's nanocomposite technology was Ube Industries, which developed a polyamide clay nanocomposite. Other polymers have been tested as matrices:[3] epoxy,[4–6] polyether,[7] and poly(ethylene oxide).[8] Polymer clay hybrids offer superior properties (high strength, high modulus, and high heat resistance[9,10]) in comparison with the original polymer. Recently, it was reported that polymer-layered silicate (clay) have the unique combination of reducing flammability and of increasing heat resistance at very low loading (2–5 wt %).[11–13]

In this article, the polyamide-6 layered-silicate prepared by melt-extrusion process is characterized in a first part, by solid-state NMR of [27]Al, ^{13}C, and wide-line ^{1}H, X-ray diffraction and TEM to determine the nanocomposite structure. In a second part, the crystallization behavior of the nanocomposite material is discussed. It is studied by differential scanning calorimetry (DSC) and by atomic force microscopy (AFM). The aim of this work is to clarify what is the precise role of the clay on the crystallization of PA-6.

EXPERIMENTAL

Materials

Raw materials used for the preparation of polyamide-6 clay hybrid (PA-6 nano) were sodium montmorillonite modified by methyl, tallow, bis-2-hydroxyethyl, quaternary ammonium chloride supplied by Southern Clay Product (Cloisite 30B) and polyamide-6 (PA-6) as pellets supplied by Rhodia (Technyl C206). Clay and PA-6 were dried 48h at 80°C before extrusion.

Preparation of polyamide-6 clay hybrid

Polymer melt-direct intercalation is an approach to make polymer layered silicate nanocomposites by using a conventional polymer extrusion process. PA-6 was melt mixed with the clay using a counterrotating twin-screw extruder (Brabender) according to conditions that permit the formation of nano-structured material.[14] The rotational speed was 300 rpm to have high shear stress, and the temperature of the five heating zones were 250°C. The extrudate was then pelletized.
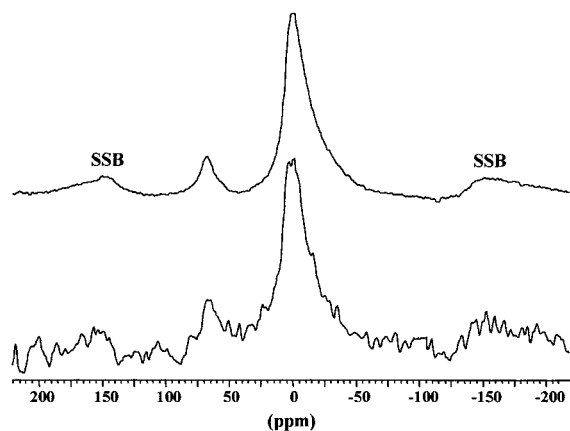
Figure 1 MAS ^{27}Al-NMR spectra of the clay (top) and of the PA-6 nano (bottom) (SSB = Spinning Side Band).

Characterization

Solid-state NMR

^{27}Al-NMR measurements were performed on a Bruker ASX400 at 104.26 MHz (9.4 T) with MAS using a 4-mm probe. A repetition time of 1 s was used for all samples. The reference used was a saturated solution of Al(OH)$_3$, and the spinning speed was 15,000 Hz. The number of scans was 1024, the pulse width was 1 μs, the spectral width was 1.25 MHz, and the acquisition time was 0.035 s, with a time domain equaling 8 ko. Lorentzian broadening equaling 100 Hz was used before Fourier transformation. Before starting a new experiment, the chemical shift reference was always verified to be within $\pm$0.2 ppm.

^{13}C-NMR measurements were performed on a Bruker ASX100 at 25.2 MHz (2.35 T) with magic-angle spinning (MAS), high-power ^{1}H decoupling (DD), and ^{1}H-^{13}C crosspolarization (CP) using a 7-mm probe. The Hartmann-Hahn matching condition was obtained by adjusting the power on ^{1}H channel for a maximum ^{13}C FID signal of adamantane. All spectra were acquired with contact times of 1 ms. A repetition time of 5 s was used for all samples. The reference used was tetramethylsilane, and the spinning speed was 5000 Hz. The number of scans was 1024, the pulse width was 3 μs, the spectral width was 20.8 kHz, and the acquisition time was 0.049 s with a time domain equaling 2 ko. Lorentzian broadening equaling 2 Hz was used before Fourier transformation. The values of chemical shift are verified using adamantane and adamantanone before starting a new experiment. For these products, the chemical shifts were within $\pm$0.2 ppm.

Proton NMR studies were carried out using a Bruker ASX 100 spectrometer, operating at a proton frequency of 100.13 MHz, with a 7-mm solenoid probe and without spinning. The method of inversion recovery [π-τ-$\pi/2$] was used to measure proton spin-lattice relaxation (T$_1$(^{1}H)) times.[15]

X-ray diffraction

XRD spectra were recorded with an automatic Siemens D5000 X-ray spectrometer using the Cu K$\alpha_{1,2}$ radiation and a nickel filter (λ = 0.15406 nm) in the range of 5° $<$ 2θ $<$ 55°. These tests were carried out on powder with a rotation of the sheets to suppress structural orientation effects.

TEM

Ultrathin section were prepared with a 45° diamond knife at room temperature using a LKB Ultrotome III ultramicrotome. Samples were embedded in an epoxy resin (Embed 812) before cutting. Thin sections (nominally 30–50 nm) were mounted on carbon-coated copper grids. Bright-field TEM images were obtained with a JEOL 100CX microscope operating at 48 kV, utilizing low-dose techniques.

Differential scanning calorimetry

Differential scanning calorimetry was carried out under nitrogen flow (5 · 10^{-7} Nm^3/s) on a Perkin-Elmer DSC-7 in aluminum pan (about 10 mg sample) from 20 to 240°C. The heating rate was 15°C/min and the cooling rate was controlled at 15°C/min. To measure the energies of crystallization and melting, In and Zn standards were used.

Atomic force microscopy

The atomic force microscopy (AFM) generates real space topographical images of a surface with both high lateral and high vertical resolution.[16] In this study, we used a Nanoscope III, from Digital Instrument Inc. in the contact mode with microfabricated Si$_3$N$_4$ cantilevers for imaging in air under atmospheric conditions according to previous published procedures.[17,18] We analyzed the surface topographical im-
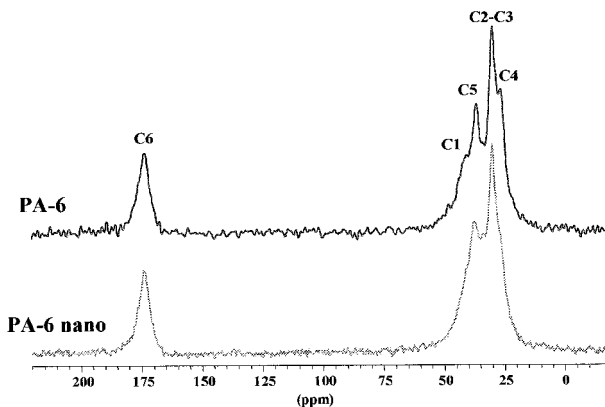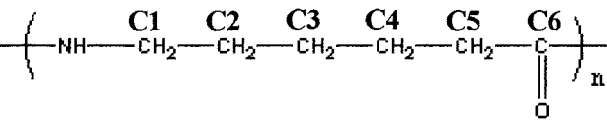

Figure 2 CP-DD-MAS ^{13}C-NMR spectra of PA-6 (top) and of the PA-6 nano (bottom).

TABLE I
Assignments of the Bands of PA-6 and PA-6nano

Repeat unit	Peaks (ppm)
$\{$—NH—$\underset{\text{C1}}{\text{CH}_2}$—$\underset{\text{C2}}{\text{CH}_2}$—$\underset{\text{C3}}{\text{CH}_2}$—$\underset{\text{C4}}{\text{CH}_2}$—$\underset{\text{C5}}{\text{CH}_2}$—$\underset{\text{C6}}{\overset{\text{O}}{\underset{\parallel}{\text{C}}}}\}_n$	(C1 α)—40.9 ppm (C2) and (C3)—29.9 ppm (C4)—26.6 ppm (C5 α)—36.5 ppm (37.3 ppm for PA-6nano) (C5 γ)—33.7 ppm (C6)—173.9 ppm

ages of PA-6 and PA-6 nano samples with image processing software, version (4.2x). A "D" head with scan area of $13 \times 13 \ \mu m^2$ was used. Sample were scanned at a constant force between 70–80 nN, with a scan rate and scan angle lying between 2.1 and 2.3 Hz and 90°, respectively, and 512 samples per area scanned.

RESULTS AND DISCUSSION

Nanocomposite structure of the polyamide-6-layered silicate

MAS ^{27}Al-NMR has a very high natural sensitivity and the ability of NMR to distinguish between AlO_4 and AlO_6 units is very informative for characterization. Figure 1 shows the MAS ^{27}Al-NMR spectra of the pure modified montmorillonite clay and of the polyamide-6-layered silicate (PA-6 nano). For the spectra, two bands can be distinguished at 60 ppm and at 0 ppm. The weak intensity's band at 60 ppm can be assigned to AlO_4 sites in the montmorillonite structure and the main resonance at 0 ppm can be assigned to AlO_6 sites in the clay.[19] This result show that the modified montmorillonite has a predominantly octahedral Al site with some tetrahedral Al. The two spectra are similar, and it indicates that the aluminosilicate layers of the clay are not chemically modified by their incorporation in PA-6 via a melt blending process.

^{13}C solid-state NMR permits one to characterize the polymers and their conformations in the solid state. It can therefore be used for determining the crystalline structure of PA-6 and PA-6 nano after extrusion.[20] PA-6 commonly crystallizes in α and γ forms.[21] The α form is the most common and thermodynamically the most stable. But in some cases, drawing or chemical treatment induce the reversible transformation of α-PA-6 into γ-PA-6.[22]

Figure 2 shows CP-DD-MAS ^{13}C-NMR spectra of PA-6 and PA-6 nano. All the bands are labeled on the spectra (five main peaks are observed corresponding to the carbons of the PA-6 repeat unit) and are assigned according to the literature (Table I).[23–25]

Additional bands (at 33.7 ppm) can be distinguished if we zoom in the region 10–60 ppm (Fig. 3). The bands at 36.5 ppm (37.3 ppm for PA-6 nano) and at

33.7 ppm can be assigned to α and γ phase of PA-6, respectively.[23,25] It means that the two polymers after extrusion at high shear stress crystallize both in α-form and γ-form. Although α-phase is thermodynamically the most stable in PA-6, some authors reported that high melt extrusion of PA-6 can contain both α and γ-crystallites.[23,25] This conclusion has been also confirmed using CP-MAS ^{15}N-NMR.[26]

To further investigate the structure of the polyamides, X-ray diffraction experiments were used. XRD patterns of PA-6 and PA-6 nano shows that the two spectra are different (Fig. 4). PA-6 nano exhibits a pronounced peak at $2\theta = 21.3°$, which can be assigned to γ-crystallites and another peak at $2\theta = 20.1°$, which can be assigned to α-crystallites.[23,25] A doublet is observed for PA-6 at $2\theta = 20.1°$ and $2\theta = 23.5°$, which is characteristic of α-crystallites. It also can be distinguished a peak at $2\theta = 21.3°$ assigned to γ-crystallites.[23,25] The results are in agreement with the NMR ones in the sense that the two kinds of crystallites (α- and γ-phase) are observed, but the conclusions are not exactly the same. Indeed, XRD indicates that α-crystallites are predominant in the case of PA-6, and that γ-crystallites are predominant in the case of PA-6 nano. NMR do not permit conclusion about the ratio between α-crystallites and γ-crystallites. This is not
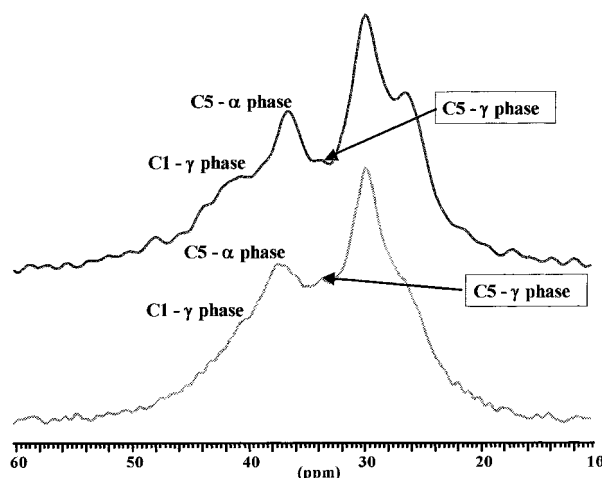

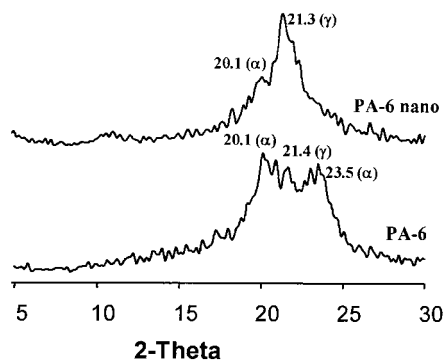**Figure 3** CP-DD-MAS ^{13}C-NMR spectra in the region 10–60 ppm of PA-6 (top) and of the PA-6 nano (bottom).

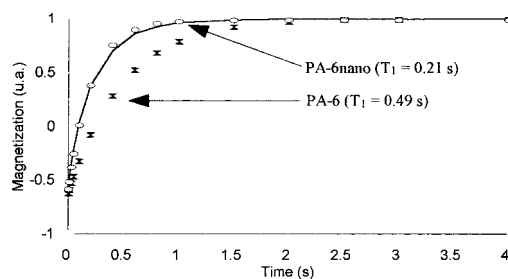**Figure 4** WXRD patterns of PA-6 (bottom) and of the PA-6 nano (top).

Figure 5 Evolution of the magnetization for an inversion–recovery experiment of PA-6 and of PA-6 nano (dots = experimental curves, plain lines = simulated curves).

surprising, because the regions of crystallinity sampled by the two techniques differ. X-ray diffraction samples the order of a crystalline environment over distances of at least 50–100 Å, while for NMR, this distance is not larger than 5–10 Å. This comparison suggests that there are crystallites both in α-form and γ-form, but that PA-6 crystallizes predominantly in α-form and PA-nano in γ-form. Recently, Mathias et al.[26] reported that the presence of nano-clay in PA-6 favored the γ-crystal and amorphous phase. They proposed that the clay surfaces induce mainly kinetically (as a controlling factor) favored formation of the γ-crystal form. That is, because the amine end groups are tightly bound to the clay surface, but not arrayed on the surface at an interchain distance that allows formation of the layered hydrogen-bonded sheets of the α-form, the γ-form is generated by default.

Polyamide-6 prepared by melt blending with modified montmorillonite clay can form two classes of nanomorphology: an intercalated or delaminated (exfoliated) structure. Wide-line solid-state NMR is used to investigate the nano structure of PA-6. According to a recent article by VanderHart et al.,[21] $T_1(^1H)$s can be used as a measure of the quality of the clay dispersion. Montmorillonite clay contains Fe^{3+}, which is strongly paramagnetic. It then is expected that the spin-exchange interaction between the unpaired electrons on different Fe atoms will produce magnetic fluctuations in the range of the Larmor frequencies for protons. The spectral density of these fluctuations is important because such phenomena will reduce $T_1(^1H)$s. For protons, if that mechanism is efficient, relaxation also propagate into the bulk of the polymer by spin diffusion. Thus, this paramagnetically induced relaxation influences the overall measured $T_1(^1H)$ to an extent that depends both on the Fe concentration in the clay layer and, on the average distance between clay layers. There is, therefore, a relationship between measured $T_1(^1H)$ values and the quality of the clay dispersion.

$T_1(^1H)$ of PA-6 and PA-6 nano are measured via inversion–recovery sequence simulating the experimental curves of magnetization (Fig. 5). $T_1(^1H)$ of PA-6

is two times higher than the one of PA-6 nano. From these data, the paramagnetic contribution, $T_{1para}(^1H)$, can be estimated as follows:[21]

$$\frac{1}{T_{1para}(^1H)} = \frac{1}{T_{1PA\text{-}6nano}(^1H)} \frac{1}{T_{1PA\text{-}6}(^1H)} = 0.37s$$

$T_{1para}(^1H)$ is dependent on spin diffusion through the bulk polymer lying between clay surfaces. According to the theory developed by VanderHart et al.,[21] a short $T_{1para}(^1H)$ is an indicator of the good exfoliation of the nanocomposite. This result suggests, therefore, that we formed an exfoliated PA-6 nano.

Direct evidence of the exfoliation of PA-6 is provided by TEM picture (Fig. 6). It is observed that the clay is well dispersed as individual nanolayers in the polymeric matrix.

Crystallization behavior of the polyamide-6-layered silicate

In a general way, the application of mechanical shear stresses during cooling from the molten state of a semicrystalline polymer promotes an orientation of the macromolecules in the direction of the material flow. This orientation can take place in the bulk material (melt spinning of synthetic fibers for instance), or mainly in the vicinity of the mould walls (injection molding). The orientation phenomenon of macromol-

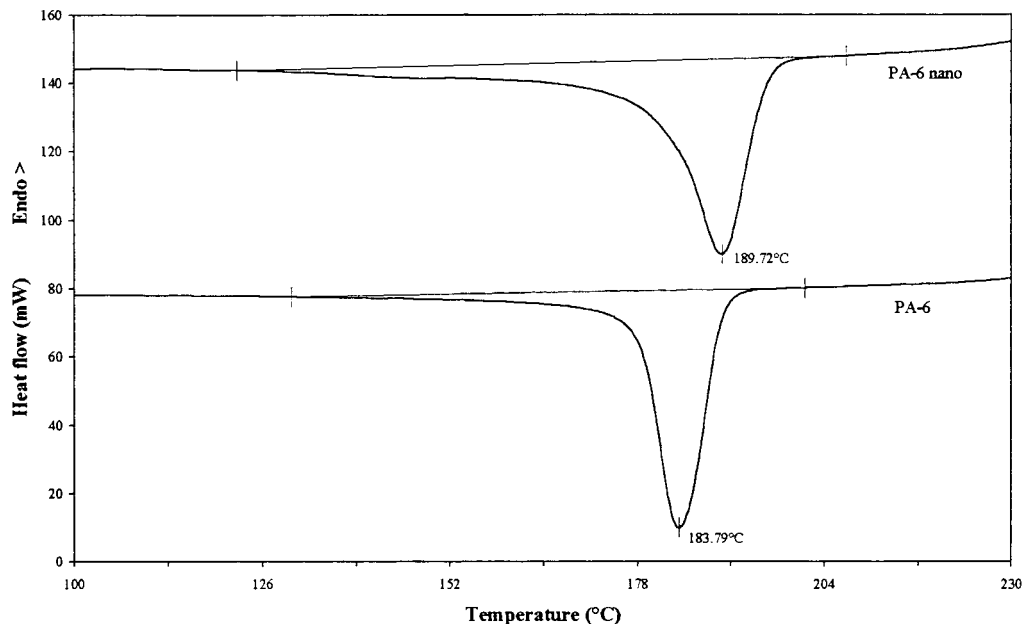**Figure 6** TEM picture of PA-6 nano.

Figure 7 Crystallization exotherms of PA-6 and PA-6 nano during cooling (15°C/min).

ecules during processing is highlighted during the subsequent polymer melting in DSC by the appearance of a complex endothermic peak. Classically, a more or less marked shoulder is observed on the endothermic melting peak at a temperature slightly lower than that of the main peak.

Polyamide 6 is a semicrystalline polymer that crystallizes in monoclinic form α or γ under suitable cooling conditions after melting of the material. The crystalline form α has a melting point around 220°C (melting point of the γ-form equals 212°C). The incorporation of nanostructures in PA-6 is processed by extrusion where the shear stresses applied to material are extremely high. For an adequate supercooling degree, these mechanical stresses cause the development of γ-form of PA-6. In addition, the appearance of the γ-form has been previously reported consecutively to the montmorillonite incorporation in the polymer during the first heating in DSC after extrusion.[27] As discussed above, it can be assigned to the presence of montmorillonite in the polymer.

To precisely control the crystallization behavior of PA-6 and to understand the precise role of montmorillonite in the process, the polymer is quickly heated to 240°C under nitrogen, then maintained at this temperature for 3 min to destroy its thermal history related to its processing and to the shear stresses generated during extrusion. The various samples are then cooled to room temperature at a controlled cooling rate of 15°C/min. Figure 7 shows the crystallization exotherms observed during cooling from the molten state of PA-6 and PA-6 nano. The exotherms maxima are located at 190 and 184°C for the polymer containing montmorillonite and for the unfilled material, re-

spectively. This behavior clearly shows the influence of clay on the polymer crystallization: after incorporation of the clay, the crystallization peak is strongly shifted towards the high temperatures. This phenomenon puts forward the role of nucleating agent played by the nanostructures. In the latter case, the polymer nucleation preferentially occurs near the montmorillonite, and a heterogeneous crystallization is favored. It is in agreement with the favored formation of PA-6 into γ-form induced clay according to the suggestion of Mathias et al.,[26] as discussed above.

After cooling from the molten state at 15°C/min without application of mechanical stresses on the material, the subsequent melting of unfilled PA-6 with a heating rate of 15°C/min shows a large endothermic peak at 220°C. The incorporation of nanostructures in PA-6 considerably modifies the melting behavior of the polymer. After crystallization of the filled polymer in the same cooling conditions, the subsequent endothermic melting peak is shifted towards the low temperatures, with a maximum around 212°C (Fig. 8). Moreover, the endothermic melting peak is complex, and a small shoulder at 220°C is observed. This behavior shows the remarkable influence of nanostructures on the PA-6 crystallization, even in the absence of mechanical stresses applied during processing. Taking into account the relative low temperature of the endotherm maximum, it is possible to link this last phenomenon to the macromolecular orientation of the polymer and to the main development of the γ crystalline form of PA-6, even without mechanical stresses applied to the polymer during its processing. This observation suggests that the macromolecules are oriented in the vicinity of the clay, which should have a
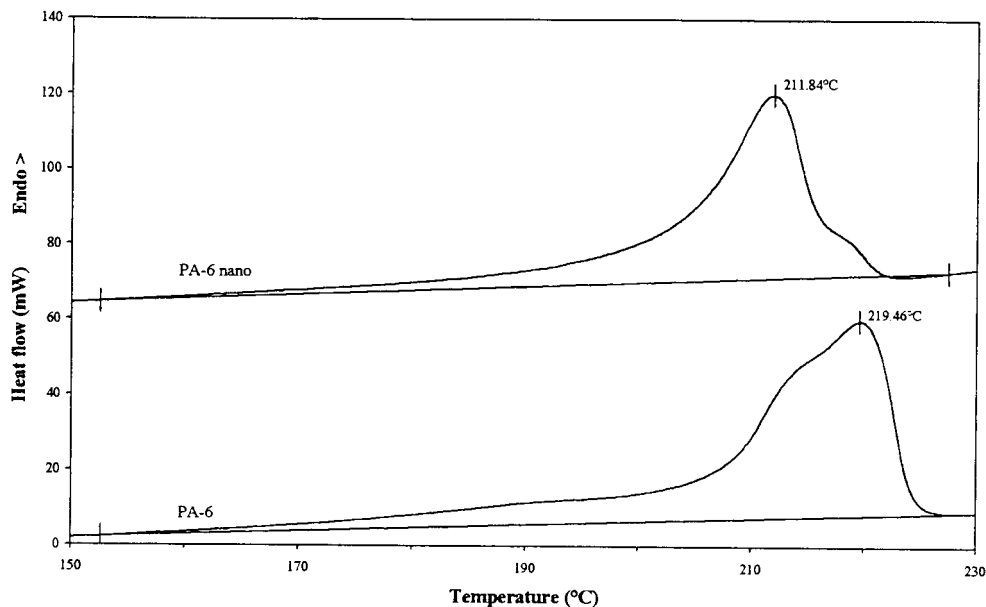
Figure 8 Melting endotherms of PA-6 and PA-6 nano during heating (15°C/min).

notable influence on the later mechanical behavior of the material. Moreover, the crystallization rate of the unfilled PA-6 differs appreciably from that of the nanocomposite material. Indeed, a melting enthalpy of approximately 60 J/g is measured in this latter case, whereas it reaches 75 J/g for the unfilled PA-6. This result shows that the crystallization rate of the nanocomposite material is definitely lower than that of the PA-6 alone when the two materials are crystallized under identical cooling conditions. This unexpected result, combined with the fact that the endothermic

melting peak develops at a lower temperature in the case of the clay hybrid polymer, shows that the polyamide macromolecules are strongly oriented in the vicinity of the clay, and do not anymore mainly crystallize in the monoclinic form.

AFM topography pictures of PA-6 nano and PA-6 after extrusion are presented on Figures 9 and 10, respectively. The surface of PA-6 nano does not show any oriented structure (Fig. 9), whereas that of unfilled PA-6 exhibits numerous spherulites (Fig. 10). This result is confirmed by TEM observation of PA-6 (Fig.
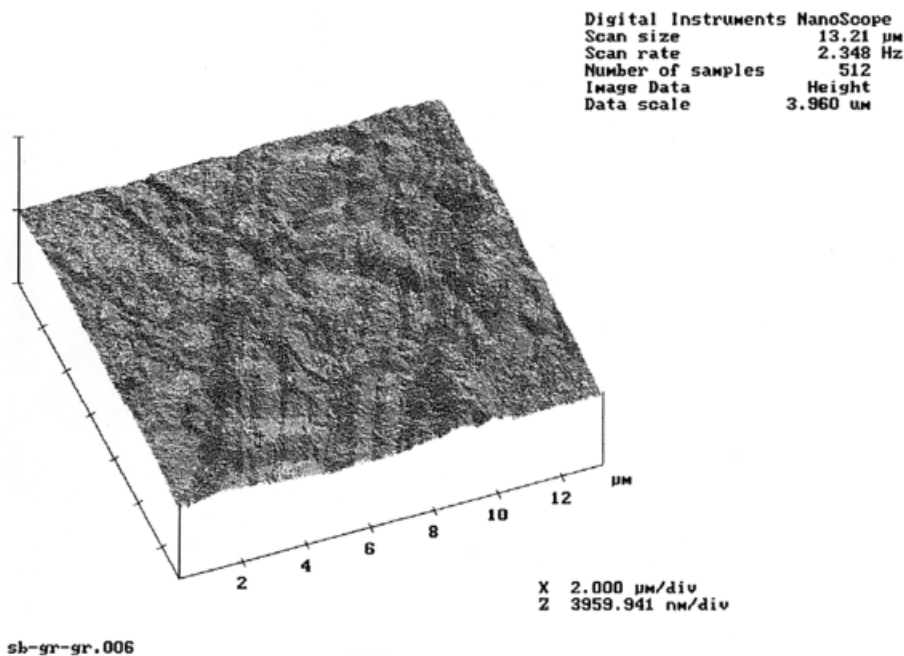


```
Digital Instruments NanoScope
Scan size              13.21 µm
Scan rate              2.348 Hz
Number of samples        512
Image Data             Height
Data scale             3.960 um
```

```
X   2.000 µm/div
Z   3959.941 nm/div
```

sb-gr-gr.006

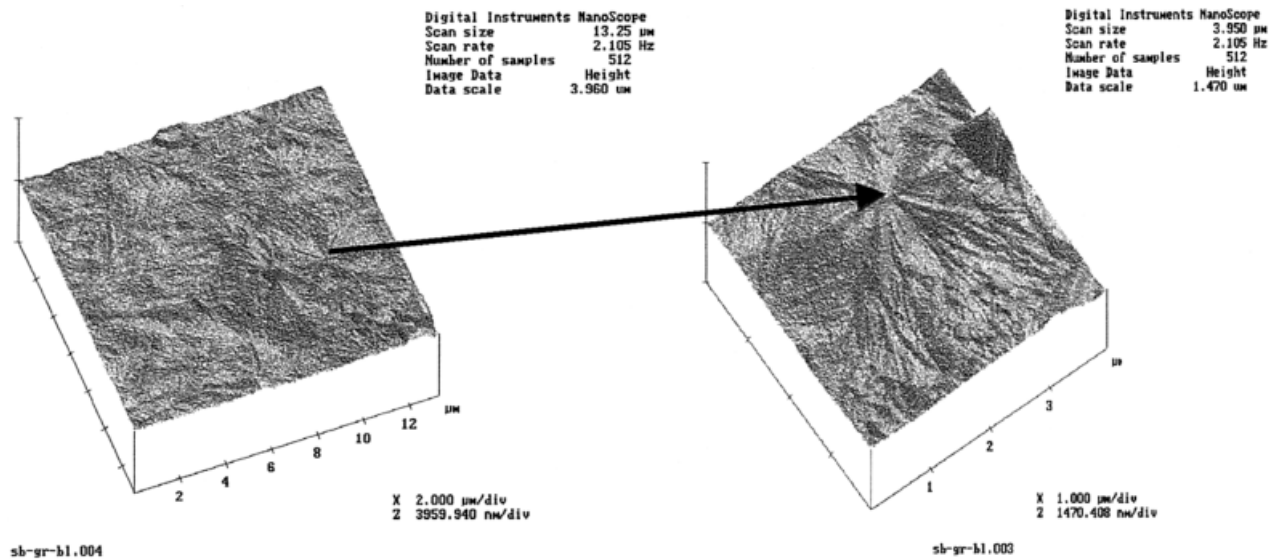**Figure 9** AFM topography picture of PA-6 nano.

Figure 10 AFM topography picture of PA-6 (a) and zoom on a spherulitic structure on the surface of PA6 (b).

11). In the processing conditions chosen for the materials extrusion, the spherulites have a diameter between 2 and 4 μm. This phenomenon clearly shows that the nanostructures play a very particular role for the polyamide crystallization. Spherulites should have indeed been observed if montmorillonite were a classical nucleating agent, with an isotropic development of the crystalline superstructures. The absence of organization of the crystalline lamellae observable at the AFM scale confirms the assumption deduced from the DSC results: polyamide macromolecules are oriented in the vicinity of the nanostructures. So, they no longer crystallize mainly in the most stable α-monoclinic system. This results in the existence of a maximum of the melting endotherm at lower temperature (212°C) than for the α-form of the polymer (220°C).

CONCLUSION

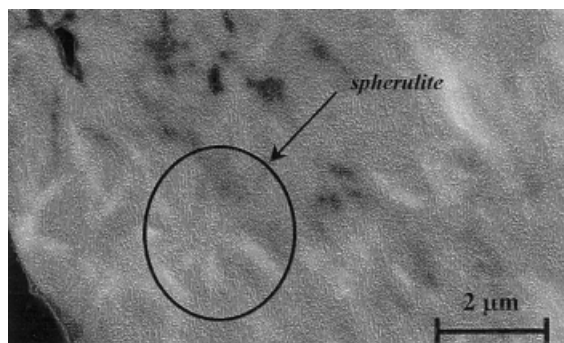Polyamide-6/clay hybrid was synthesized by melt blending at high shear stress. The nanocomposite mainly exhibits an exfoliated structure. The addition of montmorillonite-based nanostructures in polyamide 6 basically modifies the crystallization behavior of the polymer. It is shown that the modified montmorillonite induces the crystallization of PA-6 predominantly in γ-form. The presence of fillers in PA-6 increases the polymer crystallization temperature and decreases its melting point. These phenomena show that a certain number of interactions develop near the reinforcing material, and that the latter plays the particular role of nucleating agent. However, the crystallization is not spherulitic, and the assumption of macromolecular orientation in the vicinity of the clay is demonstrated by the observations carried out in DSC and AFM. These particular properties of orientation will have a particular importance on the mechanical behavior of the nanocomposite material.

Figure 11 TEM picture of PA-6 showing spherulitic structure in the bulk.

REFERENCES

1. Kohan, M. I. Nylon Plastics; John Willey & Sons: New York, 1973.
2. Modern Plastics, February 1998, p. 28.
3. Ishida, H.; Campbell, S.; Blackwell, J. Chem Mater 2000, 12, 1260.
4. Lan, T.; Pinnavaia, T. J. Chem Mater 1994, 6, 2216.
5. Messersmith, P. B.; Giannelis, E. P. Chem Mater 1994, 6, 1719.
6. Wang, M. S.; Pinnavaia, T. J. Chem Mater 1994, 6, 468.

7. Wu, J.; Lerner, M. Chem Mater 1994, 6, 835.

8. Aranda, P.; Ruiz-Hitzky, E. Chem Mater 1992, 4, 1395.

9. Giannelis, E. P. Appl Organometal Chem 1998, 12, 675.

10. Giannelis, E. P.; Krishnamoorti, R.; Manias, E. Adv Polym Sci 1999, 38, 107.

11. Gilman, J. W.; Kashiwagi, T. SAMPE J 1997, 33, 40.

12. Gilman, J. W.; Kashiwagi, T.; Giannelis, E. P.; Manias, E.; Lomakin, S.; Lichtenhan, J. D.; Jones, P. Fire Retardancy of Polymers—The Use of Intumescence; Le Bras, M.; Camino, G.; Bourbigot, S.; Delobel, The Royal Society of Chemistry: Cambridge, 1998, p. 203.

13. Gilman, J. W. Appl Clay Sci 1999, 15, 31.

14. Cho, J. W.; Paul, D. R. Polymer 2001, 42, 1083.

15. Ibbett, R.N, Ed. In NMR Spectroscopy of Polymers; Blackie Academic & Professional (an imprint of Chapman & Hall): London, 1993.

16. Binnig, G.; Quate, C. F.; Gerber, G. Phys Rev Lett 1986, 56, 930.

17. Wolff, V.; Perwuelz, A.; El Achari, A.; Caze, C.; Carlier, E. J Mater Sci 1999, 34, 3821.

18. Behary, N.; El Achari, A.; Ghenaim, A.; Caze, C. J Appl Polym Sci 2000, 75, 1013.

19. Komarnei, S.; Fyfe, C. A.; Kennedy, G. J.; Strobl, H. J Am Ceram Soc 1986, 69, 45.

20. Hatfield, G.; Glans, J.; Hammond, W. Macromolecules 1990, 23, 1654.

21. VanderHart, D. L.; Asano, A.; Gilman, J. W. Macromolecules 2001, 34, 3819.

22. Heuvel, H. M.; Huisman, R. J Appl Phys 1981, 26, 713.

23. Weeding, T. L.; Veeman, W. S.; Angad Gaur, H.; Huysmans, W. G. B. Macromolecules 1988, 21, 2028.

24. Kubo, K.; Yamanobe, T.; Komoto, T.; Ando, I.; Shiibashi, T. J Polym Sci Part B Polym Phys 1989, 27, 929.

25. Murthy, N. S.; Hatfield, G. R.; Glans, J. H. Macromolecules 1990, 23, 1342.

26. Mathias, L. J.; Davis, R. D.; Jarrett, W. L. Macromolecules 1999, 32, 7958.

27. Liu, L.; Qi, Z.; Zhu, X. J Appl Polym Sci 1999, 71, 1133.